FMRI statistical brain activation from k-space data

Daniel B. Rowe[1,2*]
[1]Department of Biophysics, [2]Division of Bistatistics,
Medical College of Wisconsin, Milwaukee, WI USA

KEY WORDS: image reconstruction, k-space, fMRI, complex data, Rowe-Logan

Abstract

In functional magnetic resonance imaging (fMRI), the process of determining statistically significant brain activation is commonly performed in terms of voxel time series measurements after image reconstruction. The image reconstruction and statistical activation processes are treated separately. In this manuscript, the relationship between complex-valued (Fourier) encoded k-space and complex-valued image measurements from (Fourier) reconstructed images is summarized. The voxel time-series measurements are written in terms of spatio-temporal k-space measurements utilizing this spatial frequency k-space and image relationship. Voxel fMRI activation can be determined in image space for example using the Rowe-Logan complex-valued activation model [Rowe, D.B., and Logan, B.R. (2004). A complex way to compute fMRI activation. NeuroImage, 23 (3):1078-1092] in terms of the original k-space measurements. Additionally, the spatio-temporal covariance between reconstructed complex-valued voxel time series can be written in terms of the spatio-temporal covariance between complex-valued k-space measurements. This allows one to utilize the originally measured data in its more naturally acquired state rather than in a transformed state. The effects of modeling preprocessing in k-space on voxel activation and correlation can then be examined.

1. Introduction

In functional magnetic resonance imaging (fMRI), an array of data for an individual image is measured in an encoded form. This measured data is generally Fourier encoded (Kumar, et al., 1975; Haacke et al., 1999) and thus are measured spatial frequencies. These spatial frequency (k-space) measurements are then reconstructed into an individual measured image array by the process of an inverse Fourier transformation. A series of these arrays of encoded images is measured and the reconstruction process is applied to each. For each voxel, temporally sequential voxel measurements are collected into a time series for determination of statistically significant activation. The originally measured spatial frequencies are complex-valued as is the inverse Fourier transformation image reconstruction process. Due to measurement error and imperfections in the Fourier encoding, voxel time series are complex-valued.

The process of determining statistical activation in each voxel has for the most part been from magnitude-only time series (Bandettini et al., 1993; Friston et al., 1994). The process of converting a complex-valued time series into a magnitude-only time series is to take the square root of the sum of the squares of the real and imaginary parts of the complex-values time series at each time point (Rowe and Logan, 2004). An activation statistic from the magnitude-only time series for each voxel is determined by computing a measure of association between the observed voxel time series and a preassigned ideal time series based on the timing of the experiment and physiological considerations. This association measure for each voxel is statistically compared to the association measure that would result from a time series of random noise. A scale of color values for the activation statistic is assigned and each voxel is given the color corresponding to its activation statistic.

The idea of computing an activation statistic from the complex-valued time series has been previously discussed (Lai and Glover, 1997; Nan and Nowak, 1999). This idea of computing fMRI activation from complex-valued data has recently been developed and expanded upon (Rowe and Logan, 2004,2005; Rowe, 2005a,b). Work has also been performed on computing fMRI activation from phase-only time series (Rowe et al., 2007b). However, the processes of image reconstruction and statistical activation have been treated separately. Additionally, activation is determined in terms of complex-valued voxel measurements after reconstruction and not the original encoded measurements.

In the current study, the relationship between the original encoded k-space measurements and reconstructed voxel measurements for each image is summarized (Rowe et al., 2007a). For each image, a vector of real-imaginary reconstructed voxel measurements is formed and written as a linear combination of real-imaginary k-space measurements. A larger vector of reconstructed real-imaginary voxel measurements is formed by stacking the individual vectors of real-imaginary voxel measurements in temporal order and written as a linear combination of a larger vector of real-imaginary k-space measurements that is formed by stacking the individual vectors of k-space measurements in temporal order. A permutation matrix as described in Appendix A is utilized to reorder

*Corresponding Author: Daniel B. Rowe, Department of Biophysics, Medical College of Wisconsin, 8701 Watertown Plank Road, Milwaukee, WI 53226, dbrowe@mcw.edu.

the voxel measurements that are real then imaginary per image to be of real then imaginary per voxel. Statistical functional brain activation can then be determined with the aforementioned recent complex-valued activation models. A map of these activation statistics can then thresholded to determine statistically significant activation while adjusting for multiple comparisons (Logan and Rowe, 2004).

Statistically significant voxel activation and correlation between voxels will now be determined in image space in terms of the originally acquired k-space measurements. This will allow the modeling of the originally acquired measurements in their original state and not in a transformed state. Implications of k-space preprocessing on voxel activation and correlation could then be evaluated.

2. Background

To aid in describing the quantitative methods of this study, a simple illustrative example is presented along with the mathematical descriptions. In MRI, the voxel intensities are not measured directly. In MRI, measurements are taken of an encoded (transformed) version of the image and the image reconstructed (inverse transformed) from the encoded measurements. The MRI encoding (transformation) is almost exclusively Fourier encoding. That is, in MRI we measure the Fourier transform of an image and reconstruct the image via an inverse Fourier transform. The Fourier transform and inverse Fourier transforms are complex-valued procedure that results in complex-valued (real-imaginary) arrays.

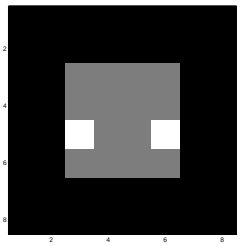

Figure 1: Ideal noiseless image.

To gain some intuition into the Fourier encoding process, consider the Fourier transform of an image that has dimensions $p_y \times p_x$. That is, p_y rows and p_x columns. Often the image is square and the number of rows is the same as the number of columns but this is not necessary. More specifically, consider an 8×8 ideal noiseless gray scale image as presented in Figure 1. Since the Fourier transform and inverse Fourier transform procedures can operate on and produce complex-valued arrays, the real-valued image in Figure 1 can be represented as a complex-valued image R_C that has a real part R_R as in Figure 1 an imaginary part R_I that is the zero matrix so that $R_C = R_R + iR_I$. The encoded or Fourier transform of this image can be found as in Equation 2.1 by pre-multiplying the $p_y \times p_x$ dimensional complex-valued matrix R_C by a complex-valued forward Fourier matrix $\bar{\Omega}_{yC} = \bar{\Omega}_{yR} + i\bar{\Omega}_{yI}$ that is of dimensions $p_y \times p_y$ and post-multiplying R_C by the transpose of another forward Fourier matrix $\bar{\Omega}_{xC}^T = (\bar{\Omega}_{xR} + i\bar{\Omega}_{xI})^T$ that is of dimensions $p_x \times p_x$ where T denotes matrix transposition. The result of the pre- and post-multiplications is a complex-valued array of spatial frequency (k-space) measurements S_C with real part S_R and imaginary part S_I as also shown in Equation 2.1.

$$(\bar{\Omega}_{yR} + i\bar{\Omega}_{yI})(R_R + iR_I)(\bar{\Omega}_{xR} + i\bar{\Omega}_{xI})^T = (S_R + iS_I) \tag{2.1}$$

This mathematical procedure is graphically illustrated in Figure 2 using the aforementioned 8×8 image. In Figure 2 the 8×8 image R_C is displayed with real part R_R given in Figure 2c and imaginary part R_I in Figure 2d is utilized to mimic a magnetic resonance echo planar imaging experiment. The spatial frequency (k-space) values S_C associated with this complex-valued image can be found by pre-multiplying the complex-valued image R_C with real image part R_R in Figure 2c and imaginary image part R_I in Figure 2d by the complex-valued forward Fourier matrix $\bar{\Omega}_{Cy}$ presented as an image with real part $\bar{\Omega}_{Ry}$ in Figure 2a and imaginary part $\bar{\Omega}_{Iy}$ in Figure 2b then post-multiplying the result by the transpose of the symmetric forward Fourier matrix $\bar{\Omega}_{Cx}$ presented as an image with real part $\bar{\Omega}_{Rx}$ in Figure 2e and imaginary part $\bar{\Omega}_{Ix}$ in Figure 2f. The spatial frequency (k-space) values S_C for the complex-valued image with real image part R_R in Figure 2c and imaginary image part R_I in Figure 2d are presented as an image with real part S_R given in Figure 2g and imaginary part S_I in Figure 2h. Note that the image does not have to be square.

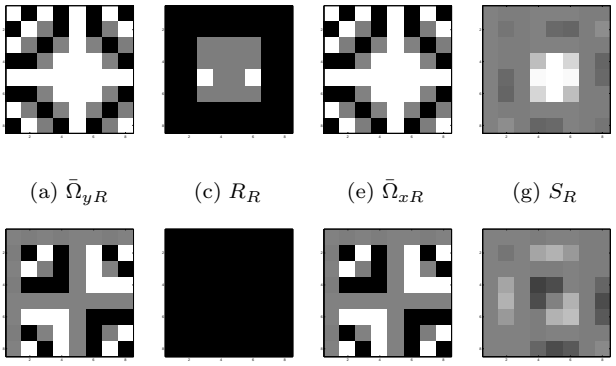

(a) $\bar{\Omega}_{yR}$ (c) R_R (e) $\bar{\Omega}_{xR}$ (g) S_R

(b) $\bar{\Omega}_{yI}$ (d) R_I (f) $\bar{\Omega}_{xI}$ (h) S_I

Figure 2: Complex-valued 2D forward Fourier transform. (a) Forward matrix real, (b) Forward matrix imaginary, (c) Image real, (d) Image imaginary, (e) Forward matrix real, (f) Forward matrix imaginary, (g) Spatial frequencies real, (h) Spatial frequencies imaginary.

However, as previously described, in MRI encoded (k-space) measurements S_C are taken and reconstructed (transformed) into an image. The inverse Fourier procedure is performed. This reconstruction procedure or inverse Fourier transform of the spatial frequency (k-space)

measurements can be found as

$$(\Omega_{yR} + i\Omega_{yI})(S_R + iS_I)(\Omega_{xR} + i\Omega_{xI})^T = (R_R + iR_I) \tag{2.2}$$

by pre-multiplying the $p_y \times p_x$ dimensional complex-valued spatial frequency matrix S_C by a complex-valued inverse Fourier matrix Ω_y that is of dimensions $p_y \times p_y$ and post-multiplying S_C by the transpose of another Fourier matrix $\bar{\Omega}_x^T$ that is of dimensions $p_x \times p_x$ where T denotes matrix transposition. The result of the pre- and post-multiplications is a complex-valued array of image measurements R_C with real part R_R and imaginary part R_I as also shown in Equation 2.2.

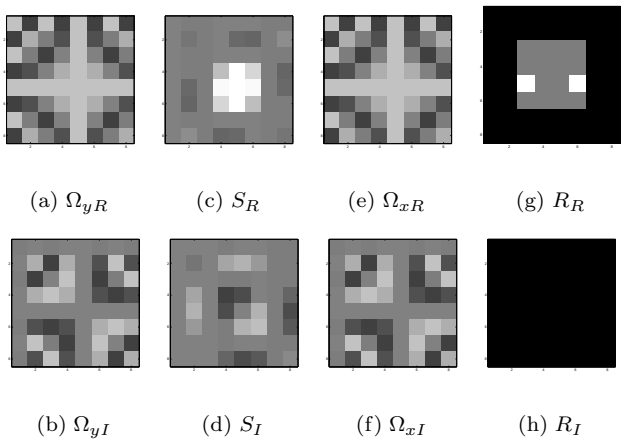

(a) Ω_{yR} (c) S_R (e) Ω_{xR} (g) R_R

(b) Ω_{yI} (d) S_I (f) Ω_{xI} (h) R_I

Figure 3: Complex-valued 2D inverse Fourier transform. (a) Inverse matrix real, (b) Inverse matrix imaginary, (c) Spatial frequencies real, (d) Spatial frequencies imaginary, (e) Inverse matrix real, (f) Inverse matrix imaginary, (g) Image real, (h) Image imaginary.

The complex-valued image R_C with real image part R_R in Figure 2c and imaginary image part R_I in Figure 2d can be recovered as seen in Figure 3. The process of recovering the original complex-valued image R_C is to pre-multiply the complex-valued spatial frequency (k-space) values S_C with real image part S_R in Figure 3c and imaginary image part S_I in Figure 3d by the complex-valued inverse Fourier matrix Ω_{Cy} presented as an image with real part Ω_{Ry} in Figure 3a and imaginary part Ω_{Iy} in Figure 3b then post-multiply the result by the transpose of the symmetric inverse Fourier matrix Ω_{Cx} presented as an image with real part Ω_{Rx} in Figure 3e and imaginary part Ω_{Ix} in Figure 3f. The recovered complex-valued image R_C is presented with real part R_R in Figure 3g and imaginary part R_I in Figure 3h.

In the above, the Fourier matrices are defined as follows. If Ω_C is a $p \times p$ Fourier matrix, it is a matrix with (j,k)th element $[\Omega_C]_{jk} = \kappa\left(\omega^{jk}\right)$ where $\kappa = 1$ and $\omega = \exp[-i2\pi(j-1)(k-1)/p]$ for the forward transformation while $\kappa = 1/p$ and $\omega = \exp[+i2\pi(j-1)(k-1)/p]$ for the inverse transformation, where $j, k = 1, ..., p$.

This complex-valued inverse Fourier transformation image reconstruction process can be equivalently described as a linear transformation with a real-valued representation often called an isomorphism in mathematics (Rowe et al, 2007a). Define a real-valued vector s to be a $2p_xp_y$ dimensional vector of complex-valued spatial frequencies from an image where the first p_xp_y elements are the rows of the real part of the spatial frequency matrix S_R in Figure 3c and the second p_xp_y elements are the rows of the imaginary part of the spatial frequency matrix S_I in Figure 3d. The real-valued vector of spatial frequencies is formed by $s = \text{vec}(S_R^T, S_I^T)$ where $S^T = (S_R^T, S_I^T)$ is a $p_x \times 2p_y$ matrix formed by joining the transpose of the real and imaginary parts of S_C as seen in Figure 4a and vec$(\cdot)$ denotes the vectorization operator that stacks the columns shown in Figure 4b of its matrix argument. This gives us a real-valued vector representation of the matrix of spatial frequency (k-space) values that is given in Figure 5b.

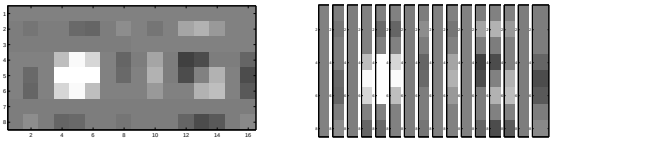

(a) Spatial frequencies S^T (b) Partitioned spatial frequencies S^T

Figure 4: Matrix to vector spatial frequency (k-space) values.

Further define a matrix Ω that is another representaion of the complex-valued inverse Fourier transformation matrices. The matrix elements of Ω are

$$\Omega_R = [(\Omega_{yR} \otimes \Omega_{xR}) - (\Omega_{yI} \otimes \Omega_{xI})] \tag{2.3}$$
$$\Omega_I = [(\Omega_{yR} \otimes \Omega_{xI}) + (\Omega_{yI} \otimes \Omega_{xR})] \tag{2.4}$$

where $\otimes$ denotes the Kronecker product that multiplies every element of its first matrix argument by its entire second matrix argument. Utilizing the complex-valued Fourier matrix Ω_{Cy} with real and imaginary parts Ω_{yR} and Ω_{yI} given in Figures 3a and Figure 3b along with the complex-valued Fourier matrix Ω_{Cx} with real and imaginary parts Ω_{xR} and Ω_{xI} given in Figures 3e and Figure 3f the resulting Ω matrix is presented in Figure 5a.

The real-valued vector representation s of the spatial frequency (k-space) values in Figure 5b is then pre-multiplied by the (inverse Fourier) reconstruction matrix Ω as in Equation 2.5

$$\begin{array}{ccccc} r & = & \Omega & * & s \\ \begin{pmatrix} r_R \\ r_I \end{pmatrix} & = & \begin{pmatrix} \Omega_R & -\Omega_I \\ \Omega_I & \Omega_R \end{pmatrix} & * & \begin{pmatrix} s_R \\ s_I \end{pmatrix} \end{array} \tag{2.5}$$

where the real-valued representation r that is of dimension $2p_xp_y \times 1$ of the complex-valued image has a true mean and measurement error.

This can be pictorially represented as in Figure 5. Figure 5b is the spatial frequency vector s and Figure 5a is the inverse Fourier transformation matrix Ω as described in Equation 2.5. This matrix multiplication produces a vector representation r of the image voxel measurements given in Figure 5c as described in Equation 2.5. The vector of voxel measurements r given in Equation 2.5 and

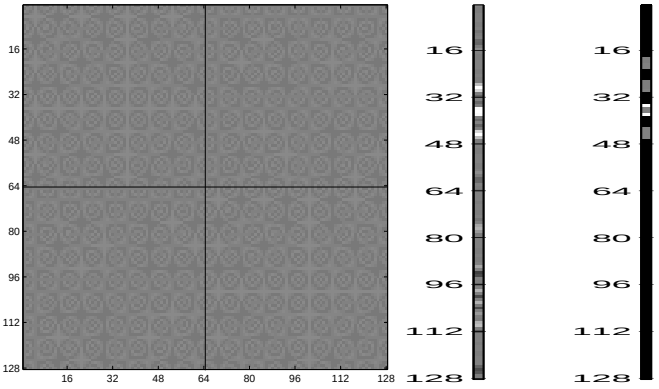

(a) reconstruction matrix Ω (b) vector s (c) vector r

Figure 5: Isomorphism for complex-valued 2D inverse Fourier Transform.

pictorially displayed in Figure 5c is partitioned into column blocks of length p_x. These blocks are then arranged as in Figure 6a and formed into a single matrix image as in Figure 6b where the first (last) eight columns are the transpose of the real (imaginary) part of the image. As can be seen, the same resultant complex-valued image is arrived at as with the complex-valued inverse Fourier transformation procedure described in Equation 2.2 and presented in Figure 3.

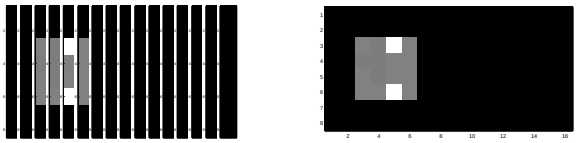

(a) partitioned image R^T (b) combined image $R^T = (R_R^T, R_I^T)$

Figure 6: Vector to matrix image values.

In the above described procedure, measurement noise was not considered. Define the $p_y \times p_x$ dimensional complex-valued spatial frequency measurement with noise to be S_C that consists of a $p_y \times p_x$ dimensional matrix of true underlying noiseless complex-valued spatial frequencies S_{0C} and a $p_y \times p_x$ dimensional matrix of complex-valued measurement error E_C. This partitioning of the measured spatial frequencies in terms of true noiseless spatial frequencies plus measurement error can be represented as

$$S_C \quad = \quad (S_{0R} + iS_{0I}) \quad + \quad (E_R + iE_I) \qquad (2.6)$$

where i is the imaginary unit while S_{0R}, S_{0I}, E_R and E_I are real and imaginary matrix valued parts of the true spatial frequencies and measurement noise, respectively. Let Ω_{Cx} and Ω_{Cy} be $p_x \times p_x$ and $p_y \times p_y$ complex-valued Fourier matrices such that

$$\Omega_{Cy} = \Omega_{Ry} + i\Omega_{Iy} \quad \text{and} \quad \Omega_{Cx} = \Omega_{Rx} + i\Omega_{Ix} \qquad (2.7)$$

where Ω_{Ry} and Ω_{Rx} are real while Ω_{Iy} and Ω_{Ix} are imaginary matrix valued parts. Then, the $p_y \times p_x$ complex-valued inverse Fourier transformation reconstructed image R_C of S_C can be written as

$$\begin{aligned} R_C &= \Omega_{Cy} * S_C * \Omega_{Cx}^T \\ &= \Omega_{Cy}(S_{0R} + iS_{0I})\Omega_{Cx}^T + \Omega_{Cy}(E_R + iE_I)\Omega_{Cx}^T \\ &= R_{0C} + N_C \end{aligned}$$

where R_C has a true mean R_{0C} and measurement error N_C. The complex-valued matrices for reconstruction Ω_x and Ω_y need not be exactly Fourier matrices but may be Fourier matrices that include adjustments for magnetic field inhomogeneities derived from phase maps or reconstruction matrices for other encoding procedures.

The real-valued inverse Fourier transformation method for image reconstruction can also be directly applied to noisy measurements. We can represent the noisy complex-valued spatial frequency matrix as $s = s_0 + \epsilon$ there these $2p_xp_y$ dimensional vectors are the reals of the rows stacked upon the imaginaries of the rows of the corresponding matrices. This implies that if the mean and covariance of the spatial frequency measurement vector s that is of dimension $2p_xp_y \times 1$ are s_0 and Γ, then the mean and covariance of the reconstructed voxel measurements r are Ωs_0 and $\Omega\Gamma\Omega^T$.

3. Methods

The previously described data for a single image is expanded upon to mimic an fMRI experiment. In fMRI, a series of the previously described slices are acquired. Denote the $p_y \times p_x$ random complex-valued spatial frequency matrix at time t as $S_{Ct} = S_{0Ct} + E_{Ct}$ and define $s_t = \text{vec}(S_{Rt}^T, S_{It}^T)$, where S_{Rt} and S_{It} are the real and imaginary parts of S_{Ct} for time points $t = 1, ..., n$. Define the total number of voxels in the image, which is the same as the number of complex-valued k-space measurements to be $p = p_xp_y$. This sequence of measured spatial frequency vectors can be collected into a $2p \times n$ matrix $S = (s_1, ..., s_n)$ where the t^{th} column contains the p real k-space measurements stacked upon the p imaginary k-space measurements for time t. Having done this, n reconstructed images can be formed by the $2p \times n$ matrix $R = \Omega S$ where the t^{th} column of R contains the p real voxel measurements stacked upon the p imaginary voxel measurements for time t, $t = 1, ..., n$.

As before, this procedure can be represented pictorially. The complex-valued image in Figure 2c and Figure 2d is taken as the mean "active" or "on" image and a duplicate of it with the two white voxels replaced by grey voxels are used as the mean "inactive" or "off" images. For illustrative purposes, a single replicate of eight on images followed by eight off images that form a single block from an experiment with eight blocks is initially presented. Subsequently all eight blocks are examined. Eight column vectors of the spatial frequencies for the true mean "on" image are joined into a matrix with eight column vectors of the spatial frequencies for the true mean "off" image as in Figure 7b. Each column

in Figure 7b is the vector form of the spatial frequencies for an image similar to that in Figure 5b.

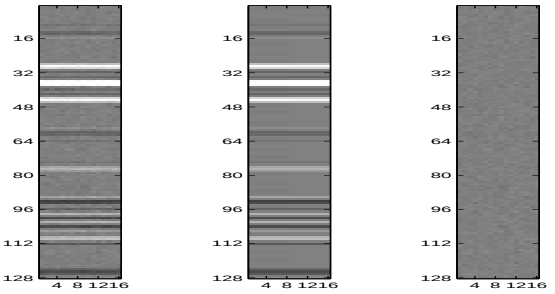

(a) noisy S (b) true S_0 (c) error E

Figure 7: Noisy spatial frequency (k-space) values.

The mean "on" images contained voxels with values $\beta_0 = 0$ and $\beta_1 = 0$ outside a four by four by four internal region, inactive gray voxels within the four by four region with values $\beta_0 = \text{SNR} * \sigma$ and $\beta_1 = 0$, along with two active voxels with value $\beta_0 = \text{SNR} * \sigma$ and $\beta_1 = \text{CNR} * \sigma$. Activation parameter values were SNR= 30, CNR= 1 and $\sigma = .05$. In this parameterization, SNR denotes the temporal signal-to-noise ratio, CNR denotes the functional contrast-to-noise ratio, and σ denotes the voxel standard deviation.

Independent noise column vectors ϵ_t as seen in Figure 7c are generated from a normal distribution with zero mean vector and covariance matrix $\Gamma = \gamma^2\ \Gamma_1 \otimes \Gamma_2 \otimes \Gamma_3$. This covariance structure mimics temporal autocorrelation along the echo planar imaging (EPI) trajectory along with correlation between real and imaginary parts. The covariance matrix was formed with Γ_1, Γ_2, and Γ_3 taken to be unit variance correlation matrices while γ was taken to be $\gamma^2 = p_x p_y\ \sigma^2$. The $p_y \times p_y$ correlation matrix Γ_1 is taken to be an AR(1) correlation matrix with $(i,j)^{th}$ element $\varrho_1^{|i-j|}$ where $\varrho_1 = 0.25$, the 2×2 correlation matrix Γ_2 is taken to have an off diagonal correlation of $\varrho_2 = .5$ while the $p_x \times p_x$ correlation matrix Γ_3 is taken to be an AR(1) correlation matrix with $(i,j)^{th}$ element $\varrho_3^{|i-j|}$ where $\varrho_3 = 0.5$.

Each matrix image in Figure 7a, b, and c was pre-multiplied by the (inverse Fourier transform) image reconstruction matrix Ω given in Equation 2.5 and presented in Figure 5a. The results of this pre-multiplication can be seen in Figure 8a, b, and c. The columns of $R = \Omega S$ in Figure 8a are real and imaginary parts for each noisy image. The noisy image in Figure 8a the sum of the noiseless image in Figure 8b and the measurement noise presented as an image in Figure 8. However, we would like real and imaginary parts for each noisy voxel. As described in Section 2, we can vectorize R and S to yield $r = vec(R)$ and $s = vec(S)$ as seen in Figure 9. The vector s of noisy spatial frequency (k-space) values as presented in Figure 9c is pre-multiplied by a block diagonal matrix with Ω along the diagonal as displayed in Figure 9b to produce a vector of noisy image measurements r as shown in Figure 9a.

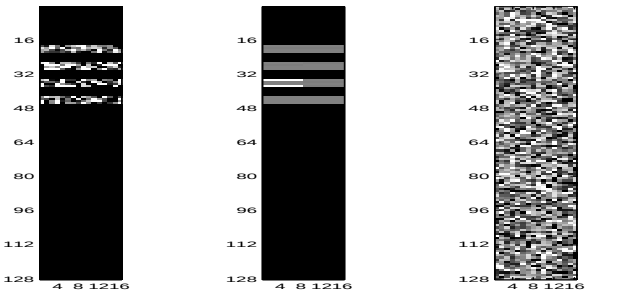

(a) noisy R=ΩS (b) true R_0=ΩS_0 (c) error N=ΩE

Figure 8: Reconstructed noisy images.

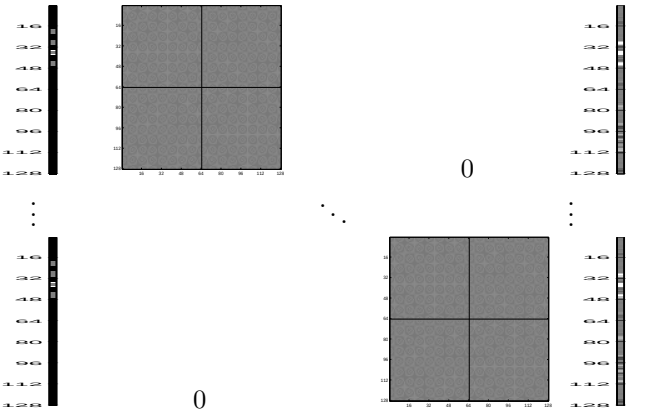

(a) noisy r (b) reconstruction matrix ($I_n \otimes \Omega$) (c) noisy s

Figure 9: Reconstructed vectorized noisy images.

The k-space measurements and the image voxel measurements can be stacked as $s = \text{vec}(S)$ and $r = \text{vec}(R)$. Note that s and r and have been redefined from their previous definition. If the mean and covariance of the $2np \times 1$ vector of spatial frequency measurements s are s_0 and Δ, then the mean and covariance of the $2np \times 1$ vector of reconstructed voxel measurements r are $(I_n \otimes \Omega)s_0$ and $(I_n \otimes \Omega)\Delta(I_n \otimes \Omega^T)$. For example, if the k-space measurements were taken to be temporally independent, then $\Delta = I_n \otimes \Gamma$ and $\text{cov}(r) = I_n \otimes (\Omega\Gamma\Omega^T)$. Thus, we have described the fMRI voxel measurements as a linear function of the fMRI k-space measurements. We can alternatively organize the voxel measurements by stacking the first set of p columns of R^T upon the second set of p columns of R^T to form a matrix Y. Having done this, the j^{th} column of the data matrix Y of dimension $2n \times p$ contains the n real voxel measurements stacked upon the n imaginary voxel measurements for voxel j, $j = 1, ..., p$. The voxel measurements Y can be described with the complex fMRI model (Rowe and Logan, 2005) as

$$Y = \left[\begin{pmatrix} C_1 X\beta_1 \\ S_1 X\beta_1 \end{pmatrix}, ..., \begin{pmatrix} C_p X\beta_p \\ S_p X\beta_p \end{pmatrix} \right] + \left[\begin{pmatrix} \eta_{R1} \\ \eta_{I1} \end{pmatrix}, ..., \begin{pmatrix} \eta_{Rp} \\ \eta_{Ip} \end{pmatrix} \right] \tag{3.1}$$

where C_1 and S_1 are diagonal matrices with cosine and sine terms respectively. Different activation models are found by different choices of the C and S matrices. The

complex constant phase model (Rowe and Logan, 2004) can be found with $C_j = I_n \cos\theta_j$ and $S_j = I_n \sin\theta_j$ where j indexes the j^{th} voxel. The unrestricted phase or magnitude only model can be found by by selecting the t^{th} element of C_j and S_j to be $C_{jt} = \cos\theta_{jt}$ and $S_{jt} = \sin\theta_{jt}$, where θ_{jt} is unique for each j and t. The complex model for both magnitude and phase (Rowe, 2005) can be found by choosing the phase $\theta_{jt} = u_t^T\gamma$ where u_t is the t^{th} row of a phase design matrix U and γ are phase regression coefficients.

This can be rearranged and written with $y = \text{vec}(Y)$ as

$$\begin{bmatrix} y_{R1} \\ y_{I1} \\ \vdots \\ y_{Rp} \\ y_{Ip} \end{bmatrix} = \begin{bmatrix} C_1X & 0 & & & 0 \\ 0 & S_1X & & & \\ & & \ddots & & \\ & & & C_pX & 0 \\ 0 & & & 0 & S_pX \end{bmatrix} \begin{bmatrix} \beta_1 \\ \beta_1 \\ \vdots \\ \beta_p \\ \beta_p \end{bmatrix} + \begin{bmatrix} \eta_{R1} \\ \eta_{I1} \\ \vdots \\ \eta_{Rp} \\ \eta_{Ip} \end{bmatrix} \quad (3.2)$$

where $y = (y_{R1}^T, y_{I1}^T, ..., y_{Rp}^T, y_{Ip}^T)^T$ is a vector containing the real and imaginary reconstructed voxel measurements and $\eta = (\eta_{R1}^T, \eta_{I1}^T, ..., \eta_{Rp}^T, \eta_{Ip}^T)^T$ is a vector containing the real and imaginary errors of the reconstructed voxel measurements. The model can be written as $y = \mu + \epsilon$. For example, with constant phase model, the mean is $\mu = (I_{2p} \otimes X)[(\cos\theta_1, \sin\theta_1) \otimes \beta_1^T, ..., (\cos\theta_p, \sin\theta_p) \otimes \beta_p^T]^T$.

The rearrangement of the voxel measurements from r to y is a linear transformation and can be achieved through a permutation matrix P (described in Appendix A) to form $y = Pr$. In terms of the original k-space measurements the voxel time courses are $y = P(I_n \otimes \Omega)\text{vec}(\text{vec}(S_{R1}^T, S_{I1}^T), ..., \text{vec}(S_{Rn}^T, S_{In}^T))$. A permutation matrix is a square matrix that can be obtained by permuting (rearranging) either the columns or rows of an identity matrix (Harville, 1999). A permutation matrix is of full rank and therefore nonsingular and also invertible. Having done this linear transformation, the mean and covariance of y are $\mu = P(I_n \otimes \Omega)s_0$ and $\Lambda = P(I_n \otimes \Omega)\Delta(I_n \otimes \Omega^T)P^T$. Since the matrices Ω and P that convert k-space measurements s to voxel measurements y are known *a priori*, the expression $y = P(I_n \otimes \Omega)s$ can be inverted to write $s = (I_n \otimes \Omega^{-1})P^{-1}y$ in terms of the parameters as

$$\begin{bmatrix} s_1 \\ \vdots \\ s_n \end{bmatrix} = \underbrace{(I_n \otimes \Omega^{-1})P^{-1}(I_{2n} \otimes X)}_{\text{Known}} \begin{bmatrix} \beta_1 \cos\theta_1 \\ \beta_1 \sin\theta_1 \\ \vdots \\ \beta_p \cos\theta_p \\ \beta_p \sin\theta_p \end{bmatrix} + \begin{bmatrix} \epsilon_1 \\ \vdots \\ \epsilon_n \end{bmatrix} \quad (3.3)$$

then the optimization for the regression coefficients (β) and phases (θ) can be performed in k-space to yield the same parameter estimates. Also note that P is an orthogonal matrix so $P^{-1} = P^T$. Activations can then be computed from Rowe's complex activation models.

Using ordinary least squares or a normal distributional specification on the errors, the voxel-wise regression coefficients and phases can be determined to yield the same point estimators as in Logan and Rowe (2004). The Rowe-Logan unconstrained alternative hypothesis estimators (with hats) for H_1: $C\beta \neq 0$ along with the constrained null hypothesis estimators (with tildes) for H_0: $C\beta = 0$ in voxel j are

$$\begin{aligned} \hat{\theta}_j &= \frac{1}{2}\tan^{-1}\left[\frac{\hat{\beta}_{Rj}^T(X'X)\hat{\beta}_{Ij}}{(\hat{\beta}_{Rj}^T(X'X)\hat{\beta}_{Rj} - \hat{\beta}_{Ij}^T(X'X)\hat{\beta}_{Ij})/2}\right] \\ \hat{\beta}_j &= \hat{\beta}_{Rj}\cos\hat{\theta}_j + \hat{\beta}_{Ij}\sin\hat{\theta}_j \\ \tilde{\theta}_j &= \frac{1}{2}\tan^{-1}\left[\frac{\hat{\beta}_{Rj}^T\Psi(X'X)\hat{\beta}_{Ij}}{(\hat{\beta}_{Rj}^T\Psi(X'X)\hat{\beta}_{Rj} - \hat{\beta}_{Ij}^T\Psi(X'X)\hat{\beta}_{Ij})/2}\right] \\ \tilde{\beta}_j &= \Psi\left[\hat{\beta}_{Rj}\cos\tilde{\theta}_j + \hat{\beta}_{Ij}\sin\tilde{\theta}_j\right] \end{aligned} \quad (3.4)$$

where C is an $r \times (q+1)$ matrix of full row rank, $\Psi = I_{q+1} - (X'X)^{-1}C'[C(X'X)^{-1}C']^{-1}C$, $\hat{\beta}_{Rj} = (X'X)^{-1}X'y_{Rj}$, and $\hat{\beta}_{Ij} = (X'X)^{-1}X'y_{Ij}$, while y_{Rj} and y_{Ij} are the $n \times 1$ vectors of real and imaginary voxel observations.

Now we can convert the vector r, displayed in Figure 9a that has values arranged that are reals and imaginaries stacked for images, to the vector y, that has values arranged that are reals and imaginaries stacked for voxels. We can convert from the vector r which is presented in Figure 9c to the vector y via a permutation matrix P. Now with the y vector being arranged as real and imaginary observations in each voxel as described in Equation 3.2, we can apply the complex activation models (Rowe and Logan, 2004). The regression coefficients β, the phase angle θ, and the variance σ^2 are estimated under both the null and alternative hypotheses as described in Equation 3.4 then activation computed. In Figures 10a and c are the unthresholded activation maps for the magnitude-only and complex-valued activation methods respectively. In Figures 10b and d are the Bonferroni 5% thresholded activation maps for the magnitude-only and complex-valued activation techniques respectively.

Voxel-wise activations will be the same as in Rowe and Logan (2004). Then the generalized likelihood ratio statistic for the complex fMRI activation model is

$$-2\log\lambda_j = 2n\log\left(\tilde{\sigma}_j^2/\hat{\sigma}_j^2\right) \ . \quad (3.5)$$

This statistic has a large sample χ_r^2 distribution. Note that when $r = 1$, two-sided testing can be done using the signed likelihood ratio test given by

$$z_j = \text{Sign}(C\hat{\beta}_j)\sqrt{-2\log\lambda_j}, \quad (3.6)$$

which has a large sample standard normal distribution under the null hypothesis. Alternatively with $r = 1$, a Wald type statistic can be formed

$$w_j = C\hat{\beta}_j/\sqrt{\hat{\sigma}_j^2 C(X^TX)^{-1}C'}, \quad (3.7)$$

which also has a large sample standard normal distribution under the null hypothesis. A map of these activation statistics is then thresholded while adjusting for multiple

comparisons (Logan and Rowe, 2004). However, correlations between voxels are characterized in terms of spatio-temporal correlations between k-space measurements.

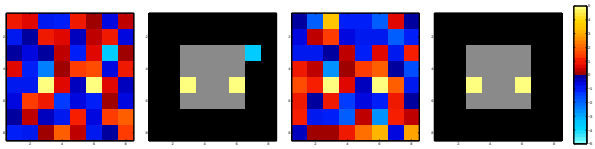

(a) Magnitude unthresholded (b) Magnitude thresholded (c) Complex unthresholded (d) Complex thresholded

Figure 10: Activation maps. Bonferroni 5% threshold.

The variances and covariances for example with a specification of uncorrelated temporal k-space measurement vectors (s_t) yields the covariance matrix $\Lambda = P(I_n \otimes \Omega\Gamma\Omega^T)P^T$ for the voxel measurements. Define the voxel measurement covariance matrix to be Σ. Having estimated the voxel-wise regression coefficients and phases, we can estimate the mean of the vector of voxel measurements y by $\hat{\mu}$ (under the alternative hypothesis) and the mean of the matrix of voxel measurements R by $\hat{M} = \overline{\text{vec}}(P^{-1}\hat{\mu})$. Here $\overline{\text{vec}}(\cdot)$ is the operator that is the inverse operation of the vec$(\cdot)$ operator. The voxel covariance matrix Σ can now be estimated by $\hat{\Sigma} = (R - \hat{M})(R - \hat{M})^T/n$.

With the physically motivated specification of the same voxel covariance Σ_W within the real-imaginary channels and voxel covariance between the real-imaginary channels Σ_B, the previous the voxel covariance matrix becomes

$$\Sigma = \begin{bmatrix} \Sigma_W & \Sigma_B \\ \Sigma_B^T & \Sigma_W \end{bmatrix}. \tag{3.8}$$

We can estimate the covariance matrices under the alternative hypothesis by

$$\hat{\Sigma}_W = \frac{(R_R - \hat{M}_R)(R_R - \hat{M}_R)^T + (R_I - \hat{M}_I)(R_I - \hat{M}_I)^T}{2n} \tag{3.9}$$

$$\hat{\Sigma}_B = \frac{(R_R - \hat{M}_R)(R_I - \hat{M}_I)^T + (R_I - \hat{M}_I)(R_R - \hat{M}_R)^T}{2n} \tag{3.10}$$

and under the null hypothesis similarly find $\tilde{\Sigma}_W$ and $\tilde{\Sigma}_B$ by replacing hats with tildes in $\hat{\Sigma}_W$ and $\hat{\Sigma}_B$.

Note that the j^{th} diagonal elements of $\hat{\Sigma}_W$ and $\tilde{\Sigma}_W$ are equivalent to those in Rowe and Logan (2004)

$$\hat{\sigma}_j^2 = \frac{1}{2n} \begin{bmatrix} y_{Rj} - X\hat{\beta}_j \cos\hat{\theta}_j \\ y_{Ij} - X\hat{\beta}_j \sin\hat{\theta}_j \end{bmatrix}^T \begin{bmatrix} y_{Rj} - X\hat{\beta}_j \cos\hat{\theta}_j \\ y_{Ij} - X\hat{\beta}_j \sin\hat{\theta}_j \end{bmatrix} \tag{3.11}$$

$$\tilde{\sigma}_j^2 = \frac{1}{2n} \begin{bmatrix} y_{Rj} - X\tilde{\beta}_j \cos\tilde{\theta}_j \\ y_{Ij} - X\tilde{\beta}_j \sin\tilde{\theta}_j \end{bmatrix}^T \begin{bmatrix} y_{Rj} - X\tilde{\beta}_j \cos\tilde{\theta}_j \\ y_{Ij} - X\tilde{\beta}_j \sin\tilde{\theta}_j \end{bmatrix}. \tag{3.12}$$

As described in Equations 2.11 and 2.12, we can also estimate covariance between voxels, $\hat{\Sigma}$. Again, note that the j^{th} diagonal element of $\hat{\Sigma}_W$ from Equation 3.9 is exactly $\hat{\sigma}_j^2$ from Rowe-Logan (2004) complex model. The sample voxel correlation from $\hat{\Sigma}_W$ described in Equation 3.9 is displayed in Figure 11a with theoretical value presented in Figure 11b. The sample correlation from $\hat{\Gamma} = \Omega^{-1}\hat{\Sigma}(\Omega^T)^{-1}$ is given in Figure 11c with theoretical value in Figure 11d. Note the similarity between the sample valuesand the theoretical values in Figures 11a and c to the theoretical values in Figures 11b and d even for the small sample size.

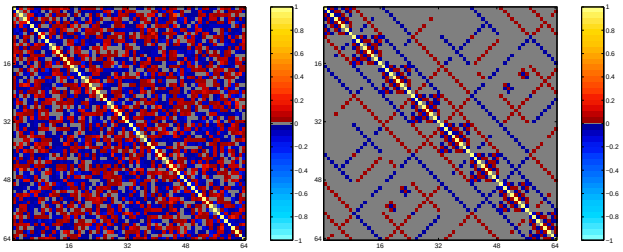

(a) sample between voxels (b) theoretical between voxels

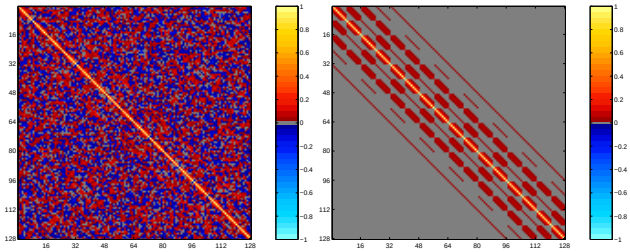

(c) sample between frequencies (d) theoretical between frequencies

Figure 11: Correlation matrices

The spatio-temporal covariances between the complex-valued voxel measurements Λ can now be described in terms of the spatio-temporal covariances between the complex-valued k-space measurements Δ. The covariance of the complex-valued k-space measurements may be due to independent sources such as spatio-temporal independent noise Δ_I and true physiologic processes Δ_P so that $\Delta = \Delta_P + \Delta_I$. Now adjustments to the k-space measurements such as shifting of alternating lines and apodization modify the correlation structure. These k-space adjustments can be written as $s_A = As = A(s_0 + \epsilon) = As_0 + A\epsilon$ and $r_A = \Omega A(s_0 + \epsilon) = \Omega As_0 + \Omega A\epsilon$ where the subscript A denotes an adjusted measurement. Then the mean and variance/covariance matrices are $\text{E}(s_A) = As_0$ and $\text{var}(s_A) = A\Gamma A^T$ for the spatial frequency measurements and $\text{E}(r_A) = \Omega As_0$ and $\text{var}(r_A) = \Omega A\Gamma A^T\Omega^T$ for the voxel measurements. So unless $\Gamma = I$ and $AA^T = I$ the voxels are correlated because $\Omega\Omega^T = I$. We are changing the physiologic and independent correlations. They change according to

$$\begin{aligned} \text{var}(s) &= \Gamma_P + \Gamma_I \\ \text{var}(s_A) &= A\Gamma_P A^T + A\Gamma_I A^T \\ \text{var}(r) &= \Omega\Gamma_P\Omega^T + \Omega\Gamma_I\Omega^T \\ \text{var}(r_A) &= \Omega A\Gamma_P A^T\Omega^T + \Omega A\Gamma_I A^T\Omega^T \end{aligned}$$

It is possible that we are missing out on or inducing correlations? We should adjust the covariance matrices.

One could apply temporal filtering or pre-whitening to the k-space measurements that are residuals after fitting a regression model in image space. After fitting the fMRI model to the voxel image time courses, we can transform the residual images into spatial frequencies (k-space) and estimate the correlation due to adjustment sources AA^T. The spatial frequencies can then be temporally pre-whitened, transformed back into residual images then the noise variation Σ_W re-estimated.

4. Discussion

Complex-valued voxel measurements have been written in terms of the original complex-valued k-space measurements. This allows the computation of statistically significant fMRI brain activation directly from the original k-space measurements but in image space. The correlation between voxel measurements can also be written in terms of correlation between k-space measurements. Since the covariance matrix between the k-space measurements and hence voxel measurements can be partitioned into individual sources of covariation, statistical associations between individual voxels or regions of interest could be quantified utilizing unmodeled sources of covariation.

Acknowledgments
Work supported in part by NIH EB00215 and AG020279.

A. Permutation Matrix

The elements of the permutation matrix P are all zero except for a single 1 in each row. The t^{th} row, $t = 1, ..., n$ within the first set of n rows of the permutation matrix P that form the n real measurements within the first voxel have a 1 in column $t = 0p + 1, 2p + 1, 4p + 1, ..., 2(n - 1)p + 1$. The t^{th} row within the second set of n rows of the permutation matrix P that form the n imaginary measurements within the first voxel have a 1 in column $t = p + 1, 3p + 1, 5p + 1, ..., 2(n - 1)p + p + 1$. The t^{th} row within the third set of n rows of the permutation matrix P that form the n real measurements within the second voxel have a 1 in column $t = 0p + 2, 2p + 2, 4p + 2, ..., 2(n - 1)p + 2$. The t^{th} row within the fourth set of n rows of the permutation matrix P that form the n imaginary measurements within the first second have a 1 in column $t = p + 2, 3p + 2, 5p + 2, ..., 2(n - 1)p + p + 2$. This general pattern continues so that the t^{th} row within the $(2p - 1)^{th}$ set of n rows of the permutation matrix P that form the n real measurements within the p^{th} voxel have a 1 in column $t = 0p + p, 2p + p, 4p + p, ..., 2(n - 1)p + p$. The t^{th} row within the second set of n rows of the permutation matrix P that form the n imaginary measurements within the first second have a 1 in column $t = p + p, 3p + p, 5p + p, ..., 2(n - 1)p + p + p$. In general, the j^{th} set of $2n$ rows for the j^{th} voxel, $j = 1, ..., p$ have a 1 in columns $0p + j, 2p + j, 4p + j, ..., 2(n - 1)p + j$ of its first n rows for the real voxel measurements and in columns $p + j, 3p + j, 5p + j, ..., 2(n - 1)p + p + j$ for the imaginary voxel measurements.

References

[1] P.M. Bandettini, A. Jesmanowicz, E.C. Wong, and J.S. Hyde. Processing strategies for time-course data sets in functional MRI of the human brain. *Magn. Reson. Med.*, 30(2):161–173, 1993.

[2] K.J. Friston, P. Jezzard, and R. Turner. Analysis of functional MRI time-series. *Human Brain Mapp.*, 1(8):153–171, 1994.

[3] E.M. Haacke, R. Brown, M. Thompson, and R. Venkatesan. *Magnetic Resonance Imaging: Principles and Sequence Design*. John Wiley and Sons, New York, 1999.

[4] D.A. Harville. *Matrix Algebra From a Statistician's Perspective*. Springer-Verlag, New York, 1999.

[5] A. Kumar, D. Welti, and R.R. Ernst. NMR Fourier zeugmatography. *J. Magn. Reson.*, 18:69–83, 1975.

[6] S. Lai and G.H. Glover. Detection of BOLD fMRI signals using complex data. *Proc. ISMRM*, 5:1671, 1997.

[7] B.R. Logan and D.B. Rowe. An evaluation of thresholding techniques in fMRI analysis. *NeuroImage*, 22(1):95–108, 2004.

[8] F.Y. Nan and R.D. Nowak. Generalized likelihood ratio detection for fMRI using complex data. *IEEE Trans. Med. Imag.*, 18(4):320–329, 1999.

[9] D.B. Rowe. Modeling both the magnitude and phase of complex-valued fMRI data. *NeuroImage*, 25(4):1310–1324, 2005a.

[10] D.B. Rowe. Parameter estimation in the magnitude-only and complex-valued fMRI data models. *NeuroImage*, 25(4):1124–1132, 2005b.

[11] D.B. Rowe and B.R. Logan. A complex way to compute fMRI activation. *NeuroImage*, 23(3):1078–1092, 2004.

[12] D.B. Rowe and B.R. Logan. Complex fMRI analysis with unrestricted phase is equivalent to a magnitude-only model. *NeuroImage*, 24(2):603–606, 2005.

[13] D.B. Rowe, C.P. Meller, and R.G. Hoffmann. Characterizing phase-only fMRI data with an angular regression model. *J. Neurosci. Methods*, 161(2):331–341, 2007b.

[14] D.B. Rowe, A.S. Nencka, and R.G. Hoffmann. Signal and noise of Fourier reconstructed fMRI data. *J. Neurosci. Methods*, 159(2):361–369, 2007a.